A BiCMOS Ultra-Wideband 3.1–10.6-GHz Front-End

Fred S. Lee and Anantha P. Chandrakasan, *Fellow, IEEE*

***Abstract*—This paper presents a direct-conversion receiver for FCC-compliant ultra-wideband (UWB) Gaussian-shaped pulses that are transmitted in one of fourteen 500-MHz-wide channels within the 3.1–10.6-GHz band. The receiver is fabricated in 0.18-μm SiGe BiCMOS. The packaged chip consists of an unmatched wideband low-noise amplifier (LNA), filter, phase-splitter, 5-GHz ISM band switchable notch filter, 3.1–10.6-GHz local oscillator (LO) amplifiers, mixers, and baseband channel-select filters/buffers. The required quadrature single-ended LO signals are generated externally. The average conversion gain and input $P_{1\mathrm{dB}}$ are 32 dB and −41 dBm, respectively. The unmatched LNA provides a system noise figure of 3.3 to 5 dB over the entire band. The chip draws 30 mA from 1.8 V. To verify the unmatched LNA's performance in a complete system, wireless testing of the front-end embedded in a full receiver at 100 Mbps reveals a 10^{-3} bit-error rate (BER) at −80 dBm sensitivity. The notch filter suppresses out-of-band interferers and reduces the effects of intermodulation products that appear in the baseband. BER improvements of an order of magnitude and greater are demonstrated with the filter.**

***Index Terms*—BiCMOS, direct conversion, low-noise amplifier (LNA), notch filter, phase-splitter, radio frequency (RF), receiver, SiGe, ultra-wideband (UWB), unmatched.**

I. Introduction

ULTRA-WIDEBAND (UWB) wireless signals were recently approved by the Federal Communications Commission (FCC) to operate in the 3.1–10.6-GHz band at a low effective isotropic radiated power (EIRP) of −41.3 dBm/MHz with a minimum signal bandwidth of 500 MHz [1]. The IEEE 802.15.3a task group is targeting UWB radios to provide wireless data rates of 480 Mbps and 1.32 Gbps at short range [2]. Though UWB signals are not considered significant interferers to narrowband systems, narrowband interferers can easily saturate a UWB front-end. This work explores the implementation and impact of an RF notch filter to improve robustness to ISM band interferers, yielding at least an order-of-magnitude improvement of bit-error rate (BER) in the presence of an interferer. Mitigating wideband noise and accounting for RF package and bond wire effects also add complexity to the integration process of a UWB receiver. This work proposes an unmatched [3] 3.1–10.6-GHz low-noise amplifier (LNA) and receiver that provides a low system noise figure (NF) of 3.3–5 dB over the entire band of operation while fitted in a quad flat no-lead (QFN) package.

Manuscript received December 1, 2005; revised March 22, 2006. This work was supported by Hewlett-Packard under the HP/MIT Alliance and by the National Science Foundation under Contract ANI-0335256.

The authors are with the Massachusetts Institute of Technology, Cambridge, MA 02139 USA (e-mail fslee@mit.edu).

Digital Object Identifier 10.1109/JSSC.2006.877270

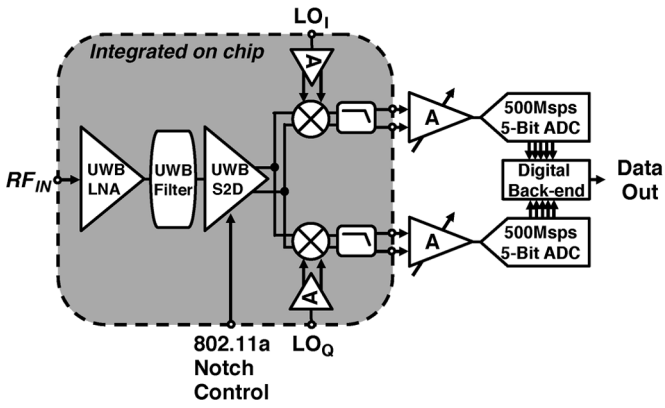

Fig. 1. Receiver architecture.

TABLE I
DYNAMIC RANGE OF INPUT SIGNALS TO RECEIVER

Signals	Power @ TX	TX-RX Distance	Power @ RX	V $_{ampl}$ @ RX
500 MHz UWB @ 3.35 GHz	-14 dBm	30 cm	-47 dBm	2.6 mV
500 MHz UWB @ 10.35 GHz	-14 dBm	10 m	-87 dBm	26 μV
802.11a @ 5.25 GHz	24 dBm	1 m	-20 dBm	30 mV
Random @ 3.1 GHz	0 dBm	1 m	-39 dBm	3.2 mV

II. System Architecture

A diagram of the receiver system that incorporates this direct-conversion RF front-end is shown in Fig. 1. The Gaussian-shaped pulses arrive in one of fourteen selectable 500-MHz-wide channels, with center frequencies denoted by $f_c = 2904 + 528 \cdot n$ [MHz], where $n = [1, 2, 3, \ldots, 13, 14]$.

Based on system analysis and simulation, 4 dB of NF is budgeted for the front-end to allow the receiver to achieve a BER of 10^{-5} in the lower sub-bands at 10 m. A maximum fixed gain of 38 dB is sufficient to handle the UWB signals listed in Table I while interfacing to a 500-Msps ADC whose full-scale input amplitude is 250 mV.

The RFIC designed in this work consists of a single-ended LNA followed by an integrated second-order high-pass filter for improved out-of-band interference rejection at minimal cost to NF. The broadband LNA is chosen as opposed to a 500-MHz sub-banded LNA [4], due to the large number of

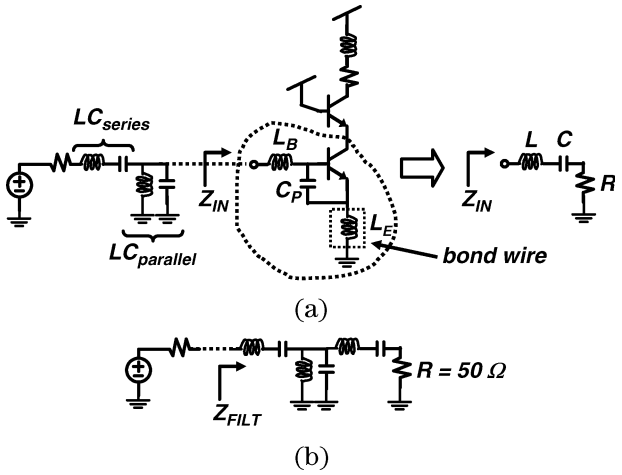

Fig. 2. (a) Ladder matched LNA and (b) third-order Chebyshev filter.

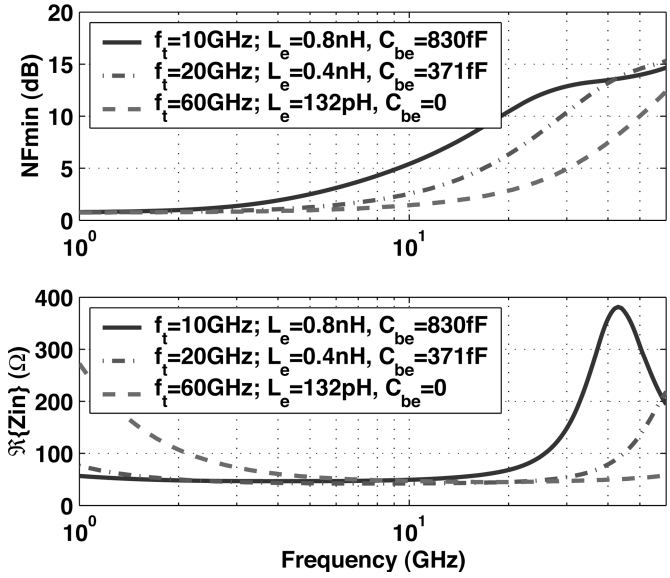

Fig. 3. (a) $\mathrm{NF}_{\min}$ and (b) $\Re\{Z_{\mathrm{IN}}\}$ of three ladder matched LNAs.

required channels across the 7.5-GHz bandwidth. However, a more feasible tradeoff to improve linearity and filtering while maintaining reasonable complexity would be to group multiple adjacent 500-MHz channels together into banks and to design an LNA that switches between these banks with a reduced number of switches and loads. The filter is followed by an RF single-to-differential converter with a switchable notch filter to suppress unwanted 5-GHz ISM signals. The single-to-differential conversion done after the LNA helps to maintain low system NF and allows the RF notch filters to be easily implemented. The mixers are degenerated double-balanced Gilbert cell mixers. The local oscillator (LO) for the mixers is generated externally. The baseband output is filtered, buffered, and interfaced to the remaining receiver chain via AC-coupling to suppress $1/f$ noise and DC offsets.

A. Low-Noise Amplifier

1) Overview: An LNA structure that achieves a broadband impedance match and good NF is the ladder matched LNA [5]. Fig. 2(a) shows the topology of such a circuit, and R is given by

$$R = 2\pi f_t \cdot L_E = \frac{g_m}{C_\pi + C_P} f \cdot L_E \tag{1}$$

where L_E is the down bond inductance and C_P is an extrinsic capacitor placed in parallel with C_π.

The structure is based upon a narrowband inductively degenerated cascode LNA that is extended to large bandwidths by adding LC_{parallel} and LC_{series} to match the topology of a third-order Chebyshev bandpass filter shown in Fig. 2(b) [6]. S_{11} of Z_{FILT} is below -10 dB for filter values that have been extracted with a tolerable ripple of less than 1 dB [7]. The NF for such a topology in SiGe is given by

$$\mathrm{NF}_{\mathrm{ladder}} = 10 \cdot log_{10}\left(1 + \frac{r_b}{Z_O} + \frac{g_m}{2} Z_O \left(\frac{w}{w_t}\right)^2\right) \tag{2}$$

where r_b and Z_O are the base resistance of the input transistor and 50 Ω of the source impedance, respectively [5]. The main feature of this topology is the ability to match the NF close to $\mathrm{NF}_{\min}$ while also achieving power match [7].

Though the ladder matched LNA provides a good input match and low NF for UWB LNAs, these specifications become difficult to maintain if the circuit is bonded to a PCB or a package. This is due to the input matching requirement depending on f_t and L_E of the circuit, as shown in (1). $\mathrm{NF}_{\min}$ for a cascode LNA is given by

$$\mathrm{NF}_{\min} = 10 \cdot log_{10}\left(1 + \frac{1}{\beta} + \sqrt{2 g_m r_b}\sqrt{\frac{1}{\beta} + \left(\frac{f}{f_t}\right)^2}\right) \tag{3}$$

where β is the current gain of the transistor.

Equation (3) shows that $\mathrm{NF}_{\min}$ is proportional to f/f_t for $f/f_t \gg \sqrt{(1/\beta)}$. Thus, if f_t must be decreased because L_E is too large to achieve a 50 Ω match (1), then the achievable $\mathrm{NF}_{\min}$ is increased. Common ways of decreasing f_t are by reducing the current density or by increasing C_P. In a packaged chip, L_E is usually constructed with a down bond whose inductance can be approximated by 1 nH/mm for $0.001''$ thick bond wires. The average length of the down bonds in this chip is 0.8 mm. Parallel down bonds can be used to reduce the inductance, but the reduction factor is limited by mutual coupling. Fig. 3 shows simulated $\mathrm{NF}_{\min}$ and $\Re\{Z_{\mathrm{IN}}\}$ of three ladder matched LNAs each intrinsically biased at an f_t of 60 GHz, and then degraded by C_P accordingly to meet the input matching requirement. The L_E inductance ranges from 132 pH and 0.8 nH. C_π for these LNAs is 170 fF. The f_t is appropriately degraded by increasing C_P for the 0.4 nH and 0.8 nH cases to maintain the input match requirement. At 10 GHz, $\mathrm{NF}_{\min}$ varies from 1.45 dB to 5.5 dB. In narrowband radio design, a solution to handle the coupled nature of $\mathrm{NF}_{\min}$ and input match consists of using two- and three-element matching networks to allow the cascode LNA to operate at a high f_t while maintaining the input match requirement. However, narrowband impedance matching structures transform impedances only across limited bandwidths and are not suitable for UWB signals. Differential LNA structures

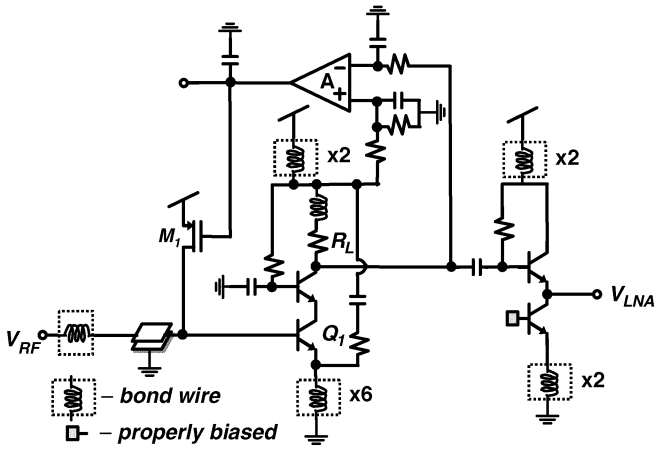

Fig. 4. Low-noise amplifier and buffer.

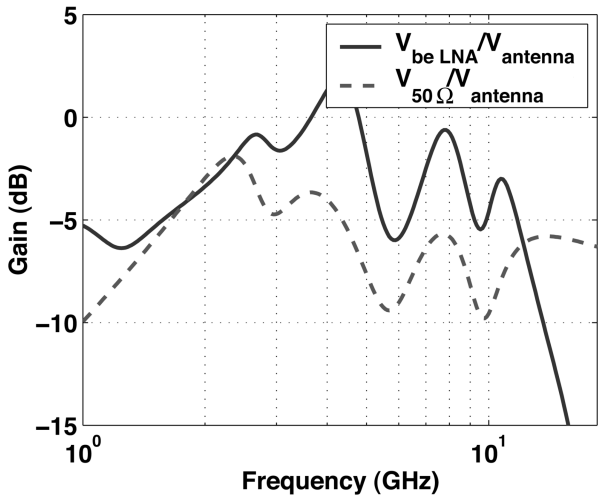

Fig. 5. Transfer functions of the antenna to a 50 Ω load and to the unmatched LNA.

that allow smaller on-chip degeneration inductors to be realized may be feasible with pre-LNA baluns, but the losses of the baluns which directly contribute to the NF of the system must be considered.

2) Unmatched LNA: To leverage the high f_t of the SiGe transistors for reduced NF, the UWB LNA here does not attempt to achieve impedance match. Instead, the inductively-peaked cascode LNA shown in Fig. 4 is viewed as a voltage amplifier and designed such that the NF to a 50 Ω source is minimized at 10 GHz, where propagation losses are greatest. Because an input match is not required, Q_1 can be biased at a high f_t for low-noise performance with minimum current. Furthermore, because the input match is not required, the lossy and noisy low-Q inductors in LC_{series} and LC_{parallel} of the ladder matched LNA are not needed. The drawback to this method is that wideband preselect filters that improve out-of-band interference rejection can no longer be used, since they require a 50 Ω match at both ports. However, this problem can be partially mitigated with a post-LNA on-chip filter and/or an LNA with sufficient linearity. To improve immunity to bond wire, package, and PCB parasitics at the LNA load, a de-Qed capacitor shunts the RF current that

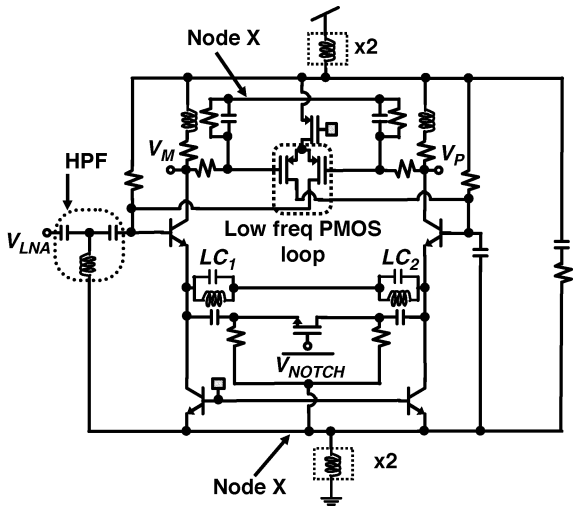

Fig. 6. Channel-select filter and single-to-differential converter.

would normally be sourced from the power supply to the low impedance ground established at the LNA emitter by parallel down bonds.

To suppress reflections due to an unmatched LNA, the antenna must be placed close to the LNA to reduce transmission line effects. The close proximity of the antenna to the IC is also desirable for minimizing cable losses that directly impact system NF. CST Microwave Studio is used to verify the antenna's transient response to an unmatched load in an electromagnetic simulator environment by replacing the receiver port with an equivalent input network of the LNA. To aid in circuit design, Spice models of the antenna are extracted from the electromagnetic simulator. Fig. 5 shows the transfer function of the extracted model to a 50 Ω matched input and to the V_{be} of the LNA input transistor.

The UWB LNA in Fig. 4 is biased with a high-impedance pMOS drain M_1 embedded in a μW feedback loop that monitors collector current through R_L and sets the g_m of Q_1. This circuit contributes minimal noise due to the large output impedance and small drain noise current of M_1. The buffer is optimized to interface the LNA to the high-pass filter and single-to-differential converter. The simulated NF of the LNA is 2–2.3 dB over the entire band, and provides a gain of 15 dB.

B. Channel-Select Filter and Single-to-Differential Converter

The channel select filter shown in Fig. 6 is formed by a three element high-pass ladder network with two capacitors and shunt inductor. The low-pass portion of the channel select filter is formed by the cascaded amplifier roll-off.

The single-to-differential converter has a cross-coupled low-frequency pMOS loop that equalizes current differences between the differential pairs to ensure balanced operation.

The switchable notch filter uses parallel LC_1 and LC_2 tanks that degenerate the emitters of the differential pair transistors with a high-impedance at their respective resonances. This reduces the gain at those frequencies. The notch frequencies are fixed at $1/\sqrt{LC}$. Any combination of LC is possible to create the filter. However, higher quality factors are obtainable with

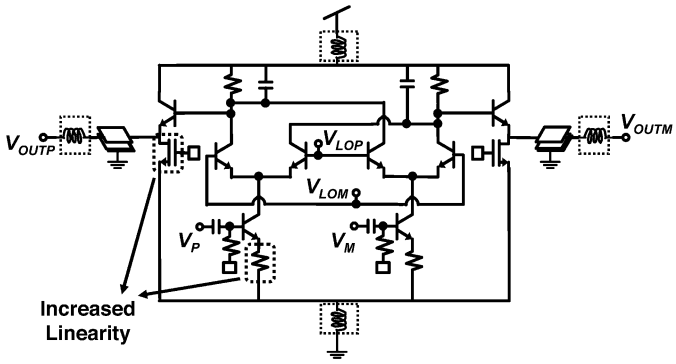

Fig. 7. Double-balanced mixer.

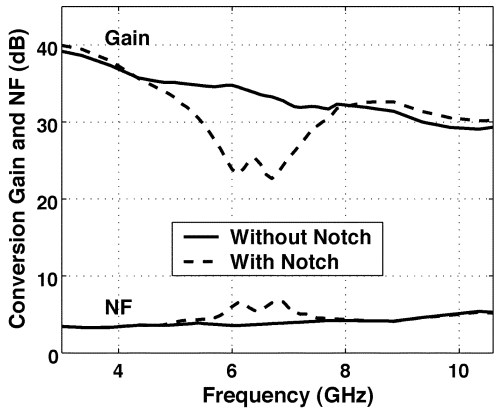

Fig. 8. Measured conversion gain and NF.

smaller inductors, thereby producing sharper notch filter characteristics. The notch frequency of each LC structure is designed at 5.25 GHz and 5.75 GHz respectively, where 5-GHz ISM signals may appear. The switch to bypass the notch filters is AC-coupled to the emitters of the differential amplifier transistor pair. This allows the switch to be reasonably sized while still having a low on-resistance because of the large overdrive. The notching and phase-splitting blocks are strategically placed after the LNA so that overall system NF is not significantly degraded.

C. Mixers and LO Amplifier Chain

The mixers are conventional double-balanced Gilbert mixers shown in Fig. 7. The RF input is resistively degenerated to increase dynamic range (DR) and linearity while decreasing the load on the previous stage. Though resistive degeneration increases the NF of the mixer, the effective increase in system NF is marginal due to the two gain stages prior to the mixer. A 250-MHz first-order low-pass filter is implemented at the output for attenuating high frequency mixing products and is assisted with a third-order off-chip filter for further channel selectivity in the system. The AC-coupling capacitors are also off-chip.

The single-ended quadrature LOs are generated off-chip through a frequency generator and a wideband I/Q phase shifter. The on-chip LO gain stages convert single-ended LO signals to differential and refine the signal through a cascade of two differential amplifiers with low common-mode gain. On-chip amplification of the LO reduces the external bond wire coupling of LO-RF and LO-LO signals.

III. Measured Results

To verify the RFIC front-end functionality, measurements of the packaged chip are reported in Section III-A. To verify the front-end in a wireless system environment, the system shown in Fig. 1 is assembled and measurements are reported in Section III-B.

A. Wired RFIC Measurements

The receiver conversion gain and NF shown in Fig. 8 are measured by sweeping the RF input from 3.1–10.6 GHz and offsetting the LO frequency by 50 MHz so that a baseband signal at 50 MHz is observed.

The average conversion gain is 32 dB and varies ± 5 dB across the bandwidth. The chip was originally designed for testing in a chip-on-board system but is packaged for robustness. The larger parasitic capacitances of the package (500 fF) and bond wire/pin inductances (2 nH) impact the RF passband. However, a system NF from 3.3 dB to 5 dB is still achieved across the 3.1–10.6-GHz bandwidth. Therefore, a flat conversion gain curve can conceivably be recovered by baseband gain compensation without degrading NF significantly. The input $P_{1\mathrm{dB}}$ increases from -46 dBm at 3.1 GHz to -36 dBm at 10.6 GHz.

When the notch filter is activated, the attenuation is 10 dB. The frequency of the notch filter is higher than expected due to over-accounted parasitics, but functionality of an RF notch in a UWB receiver system can still be examined. This filter allows the receiver to tolerate an additional 10 dB of interferer power within the notch frequencies.

To verify the front-end functionality in a full receiver, the system in Fig. 1 is implemented using the packaged RFIC front-end, external baseband gain and third-order channel-select filters, a dual 500-Msps 8-bit ADC acquisition card, and a back-end receiver built in Matlab [8]. BER measurements are made at $f_c = 3.432$ GHz and $f_c = 7.128$ GHz. Fig. 9 plots the two measured BER curves. Each non-interpolated BER point in the figure is generated by demodulating 20 packets. Each packet contains a preamble with a 31-pulse Gold code transmitted at 100 ns/pulse to achieve coarse acquisition and channel estimation, followed by 10^4 uncoded bits of data in the payload transmitted at 100 Mbps. Due to the lack of test equipment that would enable BER testing by observing millions of bits, it was not possible to measure the sensitivity for BERs $\leq 10^{-5}$. Also included in the plot is a simulated ideal BER curve for Gaussian-shaped UWB pulse signals that are limited only by additive white Gaussian noise (AWGN) and quantization noise of a 4-bit ADC. The input always spans the ADC's full scale input range and no timing offsets or pre-ADC distortion from nonlinearities that normally occur in a real front-end were included in this model [9].

For RX signals greater than -85 dBm, the maximum deviation from the ideal BER curve to the 3.432-GHz centered pulse is 3 dB. The difference in lateral translation between the BER measurements corresponds with the general increase in NF at 7.128 GHz from the NF at 3.432 GHz. For RX signals less than

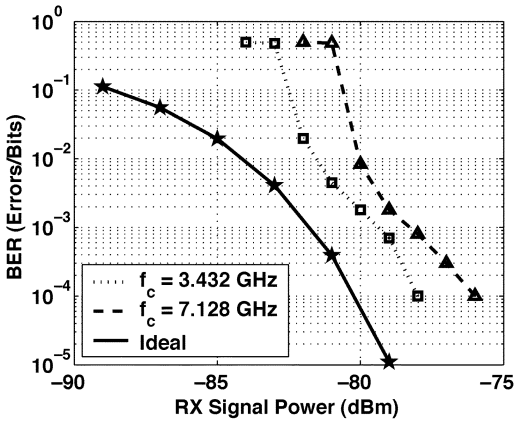

Fig. 9. Measured and simulated BER curves.

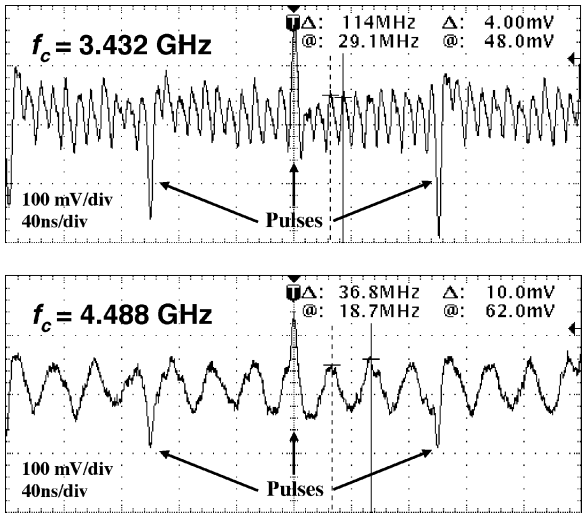

Fig. 10. Oscilloscope plot of pulses amidst IM distortion.

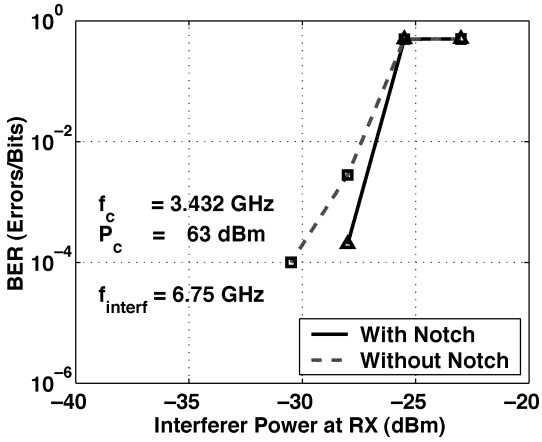

Fig. 11. Measured BER gains for 3.432-GHz pulses with the notch filter.

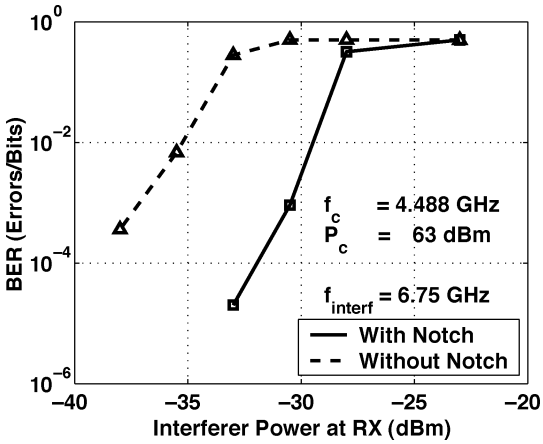

Fig. 12. Measured BER gains for 4.488-GHz pulses with the notch filter.

−85 dBm, the measured curves depart in shape from the ideal curve as they approach a BER of 0.5. This means that the signal to noise (and distortion) ratio of the system is decreasing by more than just the reduction in RX signal power.

To quantify the effectiveness of the notch filter for increasing the signal-to-interferer-plus-noise ratio (SINR) in the presence of a known interferer, BER measurements are made with two different 500-MHz-wide UWB pulses both with −63 dBm of signal power at the receiver, one centered at 3.432 GHz and another centered at 4.488 GHz. For both of these measurements, a known interferer in the notch filter band at 6.75 GHz is swept from −43 dBm to −23 dBm in 2.5 dB steps. The interferer reduces SINR by producing intermodulation (IM) products that appear in the baseband frequency with the harmonics of the LO. Fig. 10 shows the oscilloscope plots of the IM products that lie in-band. For the 3.432-GHz pulses, the 114-MHz baseband beat frequency is the IM_3 of $2 \cdot f_{\mathrm{LO}}$ and $f_{\mathrm{interferer}}$. For the 4.488-GHz pulses, the 36-MHz baseband beat frequency is the IM_5 of $3 \cdot f_{\mathrm{LO}}$ and $2 \cdot f_{\mathrm{interferer}}$. However, these unwanted IM products can be suppressed with the notch filter. Figs. 11 and 12 plot BER versus increasing interferer power, with and without the notch filter. Though the 3.432-GHz pulses are further away from the 6.75-GHz interferer than the 4.488-GHz pulses, the effect of the notch filter is greater for pulses that suffer from higher order IM products. This can be understood by observing how the IM_3 amplitude coefficient is proportional to $P_{\mathrm{interferer}}$, while the IM_5 amplitude coefficient for the 4.488-GHz pulses is proportional to $(P_{\mathrm{interferer}})^2$. By comparing the SINR improvement of Figs. 11 and 12, the one suffering from IM_3 produces a 3 dB shift between the with/without notch filter plots while the one that suffers from IM_5 produces a 6 dB shift. Correspondingly, the notch filter demonstrates one order-of-magnitude improvement in BER for the 3.432-GHz pulses and roughly four orders-of-magnitude improvement in BER for the 4.488-GHz pulses.

B. Wireless RFIC Measurements

To verify the unmatched RFIC in a wireless environment where reflections may exist, a horn antenna for wireless transmission and UWB antenna [10] for reception is added to the system configuration. Max/min gain excursions at the load due to reflections occurring in a transmission line with both ends unmatched are theoretically described by (4) and (5), where L

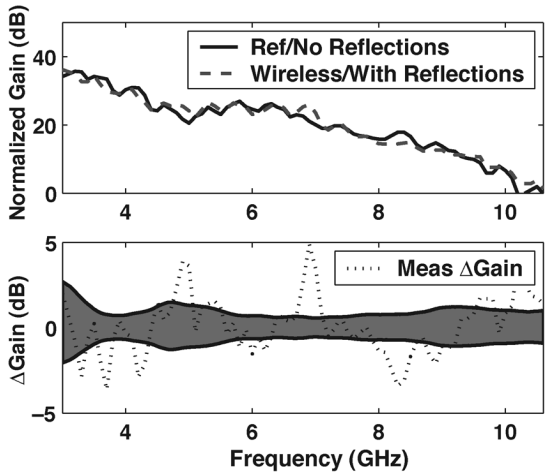

Fig. 13. (a) Normalized transfer gains. (b) Theory and measured Δgain.

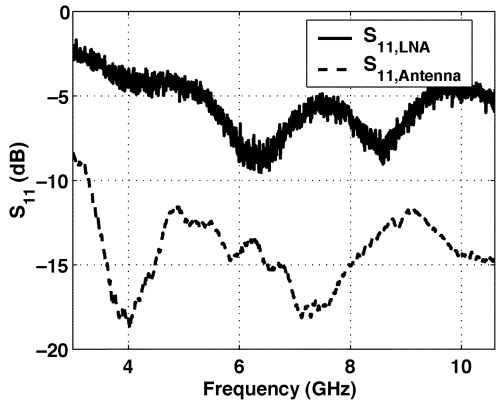

Fig. 14. Measured $S_{11,LNA}$ and $S_{11,Antenna}$.

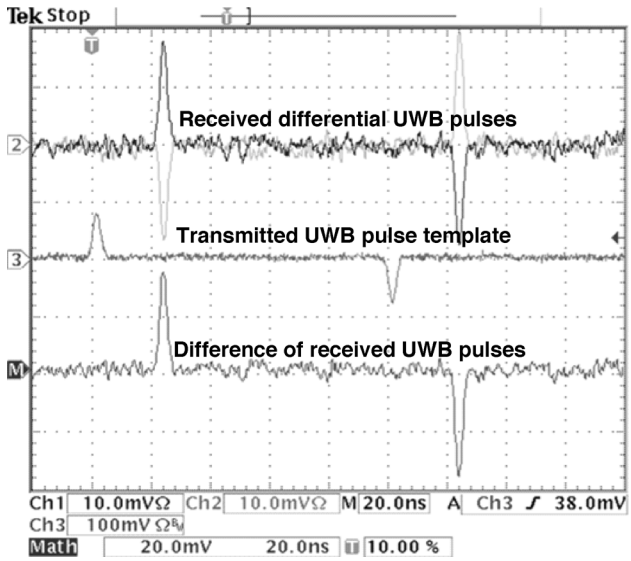

Fig. 15. Oscilloscope plot of wirelessly received UWB pulses.

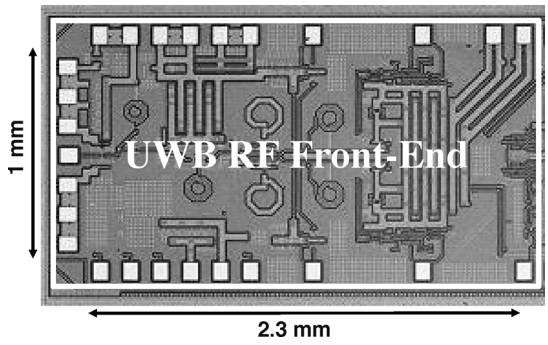

Fig. 16. Die photo.

is the loss through the transmission line and Γ is the reflection coefficient [11]:

$$A_{\max} = \frac{1}{1 - L^2 \cdot |\Gamma_{\mathrm{S11,LNA}} \cdot \Gamma_{\mathrm{S11,Antenna}}|} \tag{4}$$

$$A_{\min} = \frac{1}{1 + L^2 \cdot |\Gamma_{\mathrm{S11,LNA}} \cdot \Gamma_{\mathrm{S11,Antenna}}|}. \tag{5}$$

Fig. 13(a) is a plot of conversion gains that are normalized to the minimum gain of the wireless measurement. The reference non-wireless plot is generated by piecing together the channel loss from the TX to RX antenna and the RFIC conversion gain. Both measurements are done in reflection-less environments by ensuring at least one end of the transmission line used in each measurement is properly terminated. The total transfer gain is obtained by directly measuring the conversion gain between the TX and RX antenna/RFIC baseband output, and is subject to reflections occurring in the short transmission line between the antenna and front-end.

The total channel losses seen in Fig. 13(a) exceed what is expected from channel propagation losses [12] and measured RFIC conversion gain variations over bandwidth. The additional losses are accounted for in the reduction of the UWB antenna's azimuthal radiation pattern at higher frequencies [10].

Fig. 13(b) uses measured values of $S_{11,Antenna}$ and $S_{11,LNA}$ that are shown in Fig. 14 to plot a patch of theoretical max/min gain excursions of the system. Superimposed on this patch is a plot of the difference between the reference transfer gain without reflections and wireless transfer gain with reflections found in Fig. 13(a). The measured gain difference falls outside the boundaries within a few dB through the band while residing mostly within the boundaries otherwise. These excursions from the theoretical boundary may be due to the effective impedance of the antenna being sensitive to changing environmental factors and reflections. Though the transfer gain from antenna to LNA may fluctuate, the input signal-to-noise ratio (SNR) does not, as the changes occur uniformly to both signal and noise.

To obtain wireless BER measurements, the system is fixed 1 m apart in a line-of-sight configuration, and the transmitter power is varied to achieve the desired RX antenna power. The RX antenna power is verified with a spectrum analyzer. For RX antenna powers greater than -76 dBm, no errors were observed through 20 packets. A BER of 10^{-3} is achieved at a receiver sensitivity of -80 dBm, which matches with the wired BER measurements. An oscilloscope plot of a wirelessly received and down-converted differential pulse during coarse acquisition is shown in Fig. 15.

TABLE II
POWER CONSUMPTION AT 1.8 V

Block	**Power (mW)**
LNA	4.23
Buffer, S2D & notch	13.5
2 mixers and buffers	21.6
2 LO amplifiers	14.4
Total	**53.73**

TABLE III
CHIP PERFORMANCE SUMMARY

Specification	**Value from 3.1-10.6 GHz**
Conversion gain	39 to 29 dB
Noise figure	3.3 to 5 dB
Input P_{1dB}	-46 to -36 dBm
Notch filter attenuation	10 dB (6.25-6.75 GHz)
Sensitivity (BER=10^{-3})	-80 dBm (for 3.432 GHz pulses)
Process technology	0.18μm SiGe BiCMOS

TABLE IV
COMPARISON TABLE

Specs	**[4]**	**[13]**	**[14]**	**[15]**	**[16]**	**This work**
BW (GHz)	3 – 5	3 – 5	3 – 8	3 – 8	3 – 10	3 – 10
NF (dB)	5.5 – 8.4	4.5	5.2 – 7.7	3.3 – 4.1	4.1 – 6.2	3.3 – 5
Mean P_{1dB} (dBm)	-11	-6 (IIP3)	-10	-9.6	-23.5	-41
Power (mW)	105	195	18	238	84	54
PLL	yes	yes	no	yes	no	no
Packaged	yes	yes	no	no	yes	yes
Process	0.13 CMOS	0.25 BiCMOS	0.18 CMOS	0.25 BiCMOS	0.25 BiCMOS	0.18 BiCMOS

Table II shows the power breakdown of the front-end. A summary of chip performance is reported in Table III, and Table IV compares this UWB receiver to current work. The receiver in this work affords up to 10-GHz of sub-banded UWB pulse reception in a QFN package with low NF through the band, but linearity could be improved with a coarse gain control setting in the RF gain path and improved linearity in the mixers. The die photo of the chip is shown in Fig. 16. The active area is 1 mm $\times$ 2.3 mm.

IV. CONCLUSION

A packaged 3.1–10.6-GHz UWB RFIC front-end achieves a system NF of 3.3–5 dB over the entire band while consuming 54 mW. The single-ended quadrature LO signals are generated externally. The unmatched low-power and low-noise UWB LNA is verified within a wireless receiver system. A BER of 10^{-3} at -80 dBm sensitivity is achieved in a wireless link and is comparable to wired BER testing. A switchable -10 dB attenuation RF notch filter improves receiver SINR subject to IM distortion, thereby improving BER performance by an order of magnitude.

REFERENCES

[1] Federal Communications Commission, "Ultra-wideband transmission systems," *Federal Register*, vol. 67, no. 95, Feb. 14, 2002.

[2] IEEE 802.15.3a Task Group Website. 2005 [Online]. Available: http://www.ieee802.org/15/pub/TG3a.html

[3] J. Lerdworatawee and W. Namgoong, "Low noise amplifier design for ultra-wideband radio," in *Proc. IEEE Int. Symp. Circuits and Systems (ISCAS)*, Jun. 2003, pp. I-221–I-224.

[4] B. Razavi, T. Aytur, F.-R. Yang, R.-H. Yan, H.-C. Kang, C.-C. Hsu, and C.-C. Lee, "A 0.13 μm CMOS UWB transceiver," in *IEEE Int. Solid-State Circuits Conf. (ISSCC) Dig. Tech. Papers*, 2005, pp. 216, 594.

[5] A. Ismail and A. A. Abidi, "A 3–10 GHz low-noise amplifier with wideband LC-ladder matching network," *IEEE J. Solid-State Circuits*, vol. 39, no. 12, pp. 2269–2277, Dec. 2004.

[6] C. Bowick, *RF Circuit Design*. London, U.K.: Newnes, 1997.

[7] A. Bevilacqua and A. M. Niknejad, "An ultra-wideband CMOS LNA for 3.1 to 10.6 GHz wireless receivers," *IEEE J. Solid-State Circuits*, vol. 39, no. 12, pp. 2259–2268, Dec. 2004.

[8] R. Blazquez and A. P. Chandrakasan, "Architectures for energy-aware impulse UWB communication," in *Proc. IEEE Int. Conf. Acoustics, Speech, and Signal Processing*, 2005, pp. v/789–v/792.

[9] R. Blazquez, F. S. Lee, D. D. Wentzloff, P. P. Newaskar, J. D. Powell, and A. P. Chandrakasan, "Digital architecture for an ultra-wideband radio receiver," in *Proc. IEEE Trans. Vehicular Technology Conf.*, Oct. 2003, pp. 1303–1307.

[10] J. Powell and A. P. Chandrakasan, "Differential and single ended elliptical antennas for 3.1–10.6 GHz ultra wideband communication," in *IEEE Proc. Int. Symp. Antennas and Propagation Soc.*, Jun. 2004, pp. 2935–2938.

[11] F. S. Lee, D. D. Wentzloff, and A. P. Chandrakasan, "An ultra-wideband baseband front-end," in *IEEE Proc. Radio Frequency Integrated Circuits Symp.*, 2004, pp. 493–496.

[12] S. S. Ghassemzadeh, L. J. Greenstein, A. Kavcic, T. Sveinsson, and V. Tarokh, "UWB indoor path loss model for residential and commercial buildings," in *Proc. IEEE Trans. Vehicular Technology Conf.*, Oct. 2003, pp. 3115–3119.

[13] R. Roovers, D. M. W. Leenaerts, J. Bergervoet, K. S. Harish, R. C. H. van de Beek, G. van der Weide, H. Waite, Y. Zhang, S. Aggarwal, and C. Razzell, "An interference-robust receiver for ultra-wideband radio in SiGe BiCMOS technology," *IEEE J. Solid-State Circuits*, vol. 40, no. 12, pp. 2563–2572, Dec. 2005.

[14] G. Cusmai, M. Brandolini, P. Rossi, and F. Svelto, "An interference robust 0.18 μm CMOS 3.1–8 GHz receiver front-end for UWB radio," in *IEEE Proc. Custom Integrated Circuits Conf.*, 2005, pp. 157–160.

[15] A. Ismail and A. A. Abidi, "A 3.1–8.2 GHz zero-IF receiver and direct frequency synthesizer in 0.18 μm SiGe BiCMOS for mode-2 MB-OFDM UWB communication," *IEEE J. Solid-State Circuits*, vol. 40, no. 12, pp. 2573–2582, Dec. 2005.

[16] B. Shi and M. Y. W. Chia, "A 3.1–10.6 GHz RF front-end for multiband UWB wireless receivers," in *IEEE Proc. Radio Frequency Integrated Circuits Symp.*, 2005, pp. 343–346.

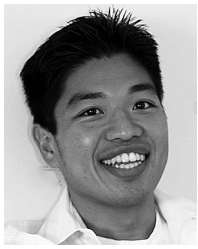

Fred S. Lee received the B.S. and M.Eng. degrees in electrical engineering and computer science from the Massachusetts Institute of Technology (MIT), Cambridge, in 2002. He is currently working toward the Ph.D. degree at MIT.

His research interests include ultra-wideband circuits and systems, CMOS/BiCMOS circuit design, low-power mixed-signal circuits, and analog RF circuit design.

Mr. Lee was a co-recipient of the DAC/ISSCC Student Design Contest Award in 2004.

Anantha P. Chandrakasan (M'95–SM'01–F'04) received the B.S, M.S. and Ph.D. degrees in electrical engineering and computer science from the University of California, Berkeley, in 1989, 1990, and 1994, respectively.

Since September 1994, he has been with the Massachusetts Institute of Technology, Cambridge, where he is currently the Joseph F. and Nancy P. Keithley Professor of Electrical Engineering. His research interests include low-power digital integrated circuit design, wireless microsensors, ultra-wideband radios, and emerging technologies. He is a co-author of *Low Power Digital CMOS Design* (Kluwer, 1995) and *Digital Integrated Circuits* (Pearson Prentice-Hall, 2003, 2nd edition). He is also a co-editor of *Low Power CMOS Design* (IEEE Press, 1998), *Design of High-Performance Microprocessor Circuits* (IEEE Press, 2000), and *Leakage in Nanometer CMOS Technologies* (Springer, 2005).

Dr. Chandrakasan has received several awards, including the 1993 IEEE Communications Society's Best Tutorial Paper Award, the IEEE Electron Devices Society's 1997 Paul Rappaport Award for the Best Paper in an EDS publication during 1997, the 1999 Design Automation Conference Design Contest Award, and the 2004 DAC/ISSCC Student Design Contest Award. He has served as a technical program co-chair for the 1997 International Symposium on Low Power Electronics and Design (ISLPED), VLSI Design'98, and the 1998 IEEE Workshop on Signal Processing Systems. He was the Signal Processing Subcommittee Chair for ISSCC 1999–2001, the Program Vice-Chair for ISSCC 2002, the Program Chair for ISSCC 2003, and the Technology Directions Subcommittee Chair for ISSCC 2004–2006. He was an Associate Editor for the IEEE JOURNAL OF SOLID-STATE CIRCUITS from 1998 to 2001. He serves on the SSCS AdCom and is the meetings committee chair. He is the Technology Directions Chair for ISSCC 2007.